A Generalized Tip-Membrane Contact Detection Algorithm for Automated Single Cell Electroporation Using Statistical Process Control

Kelly Sakaki, *Student Member, IEEE*, Hadi Esmaeilsabzali, Nikolai Dechev, *Member, IEEE*, Robert D. Burke, and Edward J. Park, *Member, IEEE*

***Abstract*—This work presents a fully automated method for detecting the contact between a microcapillary tip and a cell membrane based on a statistical process control (SPC) algorithm known as the double-sided cumulative sum (or "cusum"). By analyzing current measurements obtained through a microcapillary electrode, the proposed goal of this system is to determine when tip-to-membrane (tip-membrane) contact occurs using thin adhered cells (e.g., less than 10 μm) for the purposes of fully automated robotic-assisted, single cell electroporation (SCE)—a powerful method of gene transfection. This SPC algorithm is robust against uncontrollable system parameters such as system noise common in electrode-based systems, nonstationary processes, and variations in the physical parameters of cells. The proposed algorithm was successfully demonstrated on adhered mammal cells as small as 4 μm in thickness and using tip-placement velocities from 1 to 8 μm/s. In addition, a novel method of experimentation is described correlating optical measurements between tip-membrane proximity and changes in i_{cct} during the tip-placement sequence.**

***Note to Practitioners*—SCE by microcapillary is an efficient method to insert molecules into single cells for human health research. Before SCE can occur, placement of a microcapillary tip on a cell membrane is required. The same electrical infrastructure used for SCE is also used to detect tip-membrane contact by sensing changes in current through an electrode in the microcapillary. An abrupt decrease in current occurs during tip-membrane contact and throughout membrane indentation. By measuring this current there is no need for additional proximity sensors. In previous works, the objective was to indent the membrane sufficiently beyond the initial contact decreasing the current to a predetermined threshold—indicating the conditions required for SCE to occur. However, thin, adhered cells pose a challenge for automated tip-placement where the distance from the initial tip-membrane contact to the glass substrate is small. This limits the amount of cell indentation possible before damage to the cell and microcapillary tip occurs. In addition, the inherent noise of electrode-based systems and physical variations in thin cells, reduce the repeatability for specifying a predetermined threshold during tip-placement sequence. This work describes a system to achieve fully automated, tip-membrane contact detection of thin cells using the double-sided cumulative sum as a precursor to SCE. Little, if any, parameter modification is required for general-purpose use and this real-time, recursive algorithm can be implemented on microcontroller-based systems. This method could be extended to other electrode-based applications that are not facilitated by a microcapillary (e.g., lab-on-a-chip, microfluidic, or MEMS applications), where cell contact detection is required in the presence of a low signal-to-noise ratio.**

***Index Terms*—Automation, cusum, electroporation, microcapillary transfection, single cell, statistical process control.**

I. Introduction

AUTOMATION is becoming a vital tool for biological procedures, which are becoming increasingly complex as scientists in biotechnologies learn to exploit the unmatched capabilities of robotic-assisted single cell manipulation and analysis. Single cell electroporation (SCE) by microcapillary is a versatile and minimally invasive transfection technique that has recently been integrated into experimental automated devices for single cell manipulation. Examples of this technique include fully automated single cell manipulation and analysis systems [1], [2], and semiautomated (i.e., human-in-the-loop) systems [3]. SCE is one of the least invasive and most localized methods of transporting exogenous molecules across the cell membrane, for both *in vitro* and *in vivo* experimentation [4]–[8].

The automated tip-placement sequence for SCE places a $\sim 1\ \mu$m diameter, microcapillary tip onto the surface of the cell membrane and indents the cell. A microcapillary used in the experimental setup and the microcapillary's tip in close proximity to a cell is shown in Fig. 1(a)–(d), respectively. Electroporation is induced when an electric field at the tip-membrane interface is briefly activated at which point temporary pores form in the cell membrane. Ions and molecules contained in the microcapillary, oppositely charged from the electrode and normally impermeable to the membrane, are transported through the pores. The same circuitry used to accomplish SCE is also capable of sensing tip-membrane contact as well as providing an estimate of the SCE potential required to insert molecules through the cell membrane [5].

Manuscript received July 19, 2011; revised November 17, 2011; accepted February 03, 2012. Date of publication March 02, 2012; date of current version April 03, 2012. This paper was recommended for publication by Associate Editor Y. Sun and Editor K. Bohringer upon evaluation of the reviewers' comments. This work was supported in part by a Research Tools and Instruments Grant (EQPEQ-406188-2010) from the National Sciences and Engineering Research Council (NSERC) and in part by British Columbia Innovation Council (BCIC).

K. Sakaki, H. Esmaeilsabzali, and E. J. Park are with the Department of Mechatronic Systems Engineering, Simon Fraser University, 2 Surrey, BC V3T 0A3, Canada (e-mail: kelly.sakaki@sfu.ca; hesmaeil@sfu.ca; ed_park@sfu.ca).

N. Dechev is with the Department of Mechanical Engineering, University of Victoria, Victoria, BC V8W 3P6, Canada (e-mail: dechev@uvic.ca).

R. D. Burke is with the Department of Biochemistry and Microbiology, University of Victoria, Victoria, BC V8W 3P6, Canada (e-mail: rburke@uvic.ca).

Color versions of one or more of the figures in this paper are available online at http://ieeexplore.ieee.org.

Digital Object Identifier 10.1109/TASE.2012.2188027

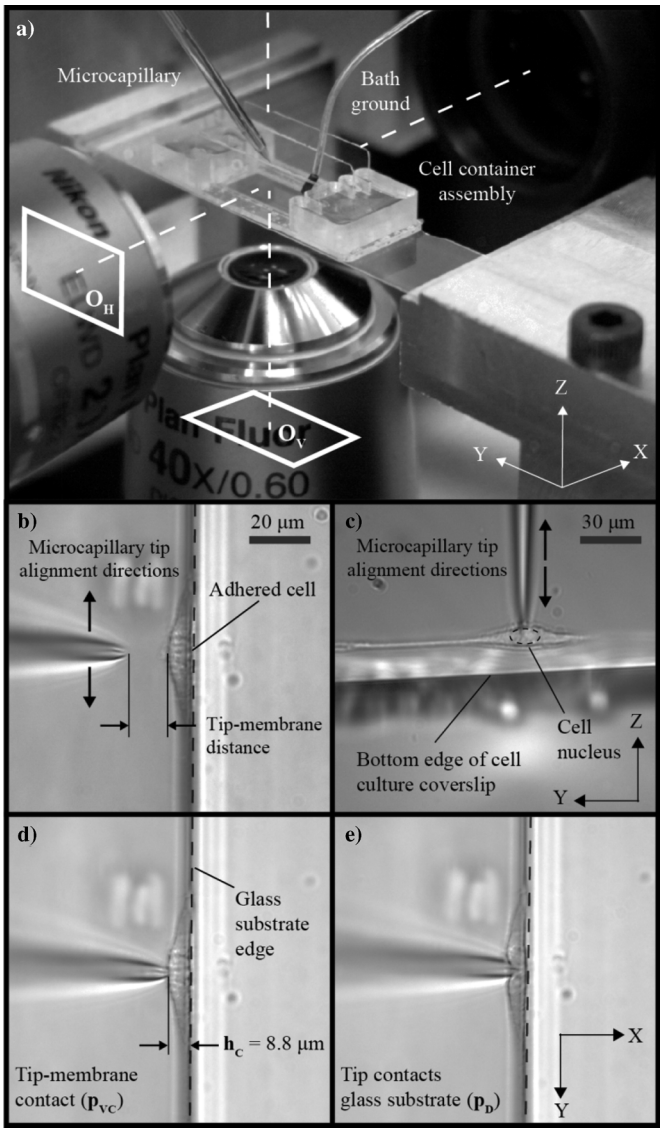

Fig. 1. Aligning the microcapillary tip to the cell. (a) The orientation relationship of the images acquired by the vertical (O_V) and the horizontal (O_H) optical trains is shown. (b) O_V provides the tip-membrane distance measure during the approach phase, P_{APR} and assists in aligning the tip to h_C on the Y axis. (c) O_H is used to align the tip to the cell nucleus on the Z axis. The alignment procedure ensures that the tip-membrane contact occurs at h_C during the tip-membrane approach sequence. (d) When tip-membrane contact occurs, a seal begins to form and a transition from P_{APR} to the indentation phase, P_{IND}, occurs at which point i_{cct} decreases abruptly. In this work, a visual estimate, p_{VC}, approximates the location of tip-membrane contact p_C. (e) At 100% indentation, the tip contacts the substrate at p_D, the cell is destroyed and the tip is damaged.

The high selectivity of automated microcapillary-based methods of cell manipulation such as SCE [1], [3], cell aspiration [9], pronuclear, and intracytoplasmic injection [10], [11] allows individual cells or small features [6] on cells to be targeted for single cell manipulation methods. Cells in suspension can be held in place with a holding microcapillary and injected with a second microcapillary, while existing on the same focal plane. This is beneficial since it can allow effective real-time visual processing (i.e., visual servoing) as well as tip-membrane feedback (e.g., force-feedback [12].

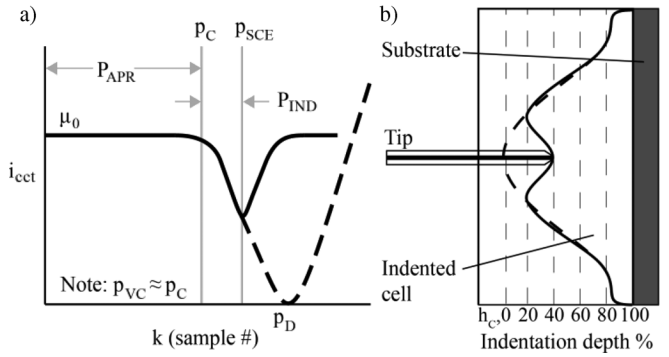

Fig. 2. (a) An ideal representation of i_{cct} is shown as the tip approaches the cell membrane. Samples, k, are time-invariant and the approach velocity of the tip is constant. At p_C, tip-membrane contact occurs. The tip halts after some indentation of the membrane (P_{IND}), where SCE would be initiated (p_{SCE}). The tip is retracted and the i_{cct} returns to the original value (solid line). If the motion of the tip is not stopped, the tip makes contact with the glass substrate (dashed line) at p_D. (b) The "indentation depth%" is the amount of indentation relative to the initial point of contact of the tip to the membrane, h_C, common to all of the cells (i.e., 0% indentation depth). In the figure 40% indentation depth is shown.

This work considers the case of adhered cell lines where the height of the cell, h_C (thickness of the cell normal to the substrate) is relatively small (e.g., less than 10 μm) and the tip and desired target on the cell exist on the same focal axis (e.g., top-down delivery method). Such cells, using this method of delivery, exhibit an absence of discernable visual information on the Z axis, which severely limits the accuracy of visual cues to determine the distance between the tip and the cell membrane for automated, machine vision techniques. Therefore, information concerning the tip-membrane contact detection method must comes from other sources of feedback such as amplitude changes of a low potential, bipolar square wave signal representing the current through the micropipette electrode i_{cct}.

One of the major tasks and a precursor to automating SCE is to successfully detect the point when sufficient tip-membrane contact is made at which point an effective seal is created between the tip and the membrane prior to SCE. The trend of i_{cct}, during the tip-placement sequence, is represented by μ_0, the average measurement of i_{cct} [the solid line in Fig. 2(a)]. μ_0 is relatively constant during the approach phase, P_{APR}. When the tip first contacts the membrane at p_C (i.e., 0% indentation depth shown in Fig. 2(b), the formation of a seal between the tip and the surface of the cell membrane begins to form and the indentation phase, P_{IND} begins. As the depth of indentation increases, i_{cct} decreases rapidly. When "sufficient" tip-contact is made, motion of the microcapillary tip is halted at p_{SCE}, and SCE is initiated briefly. The tip then returns to the original position before P_{APR} was initiated for further cell manipulations. If the motion of the microcapillary is not stopped prior to reaching the glass substrate, p_D (i.e., 100% indentation depth), the tip is damaged, the cell will rupture, and a large increase in i_{cct} is observed after p_D [dashed line in Fig. 2(a)]. Images from a tip-membrane placement sequence are shown including: the tip-membrane approach phase, P_{APR} [Fig. 1(b)]; the tip at the visually estimated point of contact, p_{VC} [Fig. 1(d)] and the tip in contact with the glass substrate, p_D [Fig. 1(e)].

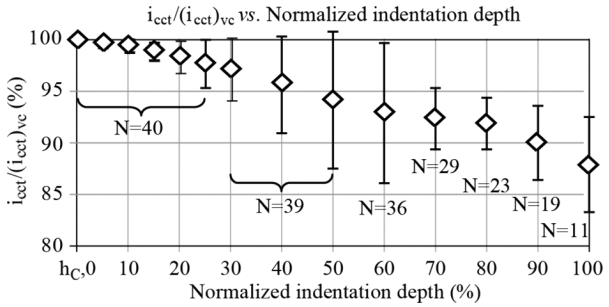

Fig. 3. The change in the ratio of $i_{cct}/(i_{cct})_{vc}$ as the membrane is indented by the tip using the current, $(i_{cct})_{vc}$, measured at p_{VC} as the initial reference. The number of cells, N, available decreases after 70% indentation depth due to the cell rupturing or tip-breakage near 100% indentation. The number of trials was 40, and the values of i_{cct} were estimated using a moving average (window size $= 16$).

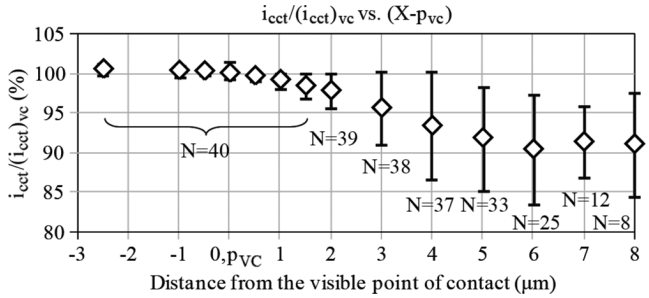

Fig. 4. The measured value of i_{cct} with respect to locations relative to p_{VC}. The number of trials was 40, and the values of i_{cct} were estimated using a moving average (window size $= 16$).

The change in i_{cct} due to the tip-membrane proximity and the degree of indentation (i.e., formation of the seal) is measured between the two electrodes: one within the microcapillary and the other in the cell bath. This change provides a measurable quantity necessary for the tip-membrane contact detection [5]. However, difficulties arise when the tip-placement is attempted on cells with a small h_C, and where the system is required to react quickly to a small, abrupt change in i_{cct}, which is only several times greater than the signal-to-noise ratio (SNR). The SNR, with respect to the desired detectable shift can be defined as

$$\mathrm{SNR} = \frac{\mu_1 - \mu_0}{\sigma} \tag{1}$$

μ_1 is the shifted level above or below μ_0. Subsequently, smaller shifts suffer from a lower SNR and are more difficult to detect. The low SNR and small h_C limit the available indentation depth during P_{IND}, increasing the chance of damage to the cell or tip. In this application, the i_{cct} measurement standard deviation, σ, is representative of the system noise, which randomly alternates about μ_0. Noise is typically induced from common system sources including electromechanical devices and power sources. However, noise recorded from electrode-based systems is significant and is greater when a tip-membrane seal is not formed [13].

Indenting thin adhered cells (e.g., NIH/3T3 mouse fibroblasts), the cell-to-cell variability of $i_{cct}/(i_{cct})_{VC}$, representing the current through the electrode with respect to the current at p_{VC}, is high. For example, at 50% indentation depth, the average $i_{cct}/(i_{cct})_{VC}$ for all of the cells tested reduced to 94.2% (SD 6.6%, N 39–Fig. 3). At an average indentation depth of 4 μm from the p_{VC} (i.e., slightly greater than half the average thickness of the cells measured) the average $i_{cct}/(i_{cct})_{VC}$ reduced to 93.4% (SD 6.8%, N 37–Fig. 4). In Figs. 3 and 4, the number of cells, N decreases significantly after 70% indentation depth due to the cell rupturing or tip-breakage near 100% indentation. The total number of trials used during the offline analysis was 40.

In prior work [1], [3], the objective of the tip-placement procedure is to reach a current threshold corresponding to the voltage level required for molecules to be transferred from the microcapillary to the cell to achieve SCE [5]. However, the high variation in the result illustrated in Figs. 3 and 4, suggest that cells with a thickness comparable to the NIH/3T3s require a better method for the tip-placement procedure. Cells with a larger h_C can accommodate a greater indentation (i.e., larger i_{cct} threshold), and are, therefore, more likely to achieve a common threshold with less possibility of damage to the tip or to the cell. Conversely, setting current thresholds too low for smaller indentation depths will result in false contact alarms due to noise fluctuations and may prevent tip-membrane contact from occurring. Therefore, specification of a general threshold to achieve efficient placement of the tip for thin cells is nontrivial and is difficult to estimate in general.

The versatility of SCE by microcapillary and the widespread use of electroporation in biotechnology potentially provide a powerful, automated method of processing. However, all of the phases required in fully automated SCE including the detection of the transition from P_{APR} to P_{IND} (i.e., tip-membrane contact) must be effectively generalized to target not only large cells, but also thin adhered cell lines. A fully automated means of the tip-membrane contact detection, facilitating limitations caused by system noise and cell variations has yet to satisfy this task level requirement and thus is the focus of this work. The combination of irregular shape mammalian cells with a small h_C, low SNR, and a lack of reliable visual information requires an early warning to indicate the initial tip-membrane contact and avoid: (i) a false threshold detection leading to an insufficient tip-membrane placement; (ii) the destruction of the tip; and/or (iii) the destruction of the cell.

In this application, the relatively constant current level during P_{APR}, the random noise about μ_0 and the abrupt change in i_{cct} at p_C make SPC methods, such as the cusum, an effective method for quickly detecting small shifts in μ_0 in a low SNR environment. Therefore, if the i_{cct} measurements can be processed such that tip-membrane contact is reliably detected over a short indentation depth in the presence of random noise, a repeatable indicator for the tip-membrane contact can be generalized for cells with both large and small h_C satisfying the goals of this work. Following the tip-membrane detection, the potential required for electroporation can be adjusted based on the estimated change in i_{cct} to meet the requirements for SCE to occur; however, is not the focus in this work.

This work includes five sections. Section I provides a background and a description of the challenges of automated SCE

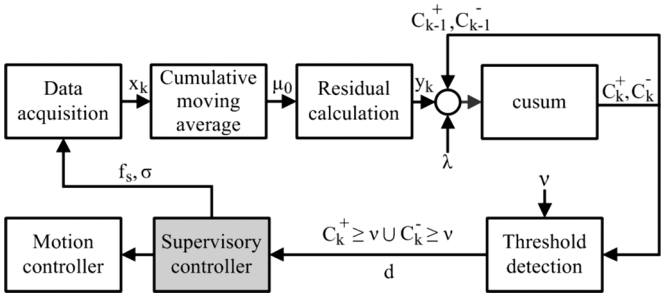

Fig. 5. The system diagram. The data acquisition module outputs the raw data, which updates the cumulative average and the residuals. The threshold is tested to determine the status of the tip-placement sequence. The motion controller responds to directives issued by the supervisory controller, which receives an alarm notification from the threshold detector regarding tip-membrane contact or tip-breakage.

of thin cells. In Section II, the data acquisition method is presented, and an explanation of the proposed system algorithm for the completion of the objectives of this work is provided. Section III provides a description of the experimental setup used to correlate i_{cct} with the visual estimate of tip-membrane position. Section IV provides the results and a discussion of the offline analysis and online results used to demonstrate the algorithm. Finally, Section V concludes this work.

II. Methodology

Statistical methods of change detection are used frequently in a wide range of statistical processes and quality control applications (e.g., [14] and [15]). Their purpose is to detect abrupt changes or provide an early warning of changes to the system parameters that change rapidly [16].

A. Automated System for i_{cct} Change Detection

With respect to automated SCE, an early indication of the P_{APR} to P_{IND} transition can minimize the initial depth of indentation and reduce the possibility of damage to the microcapillary tip or to the cell. In addition to monitoring i_{cct} for the tip-membrane contact, i_{cct} should also be monitored for damage to the microcapillary tip during P_{IND} such as tip-breakage. Therefore, it is desirable to monitor for the occurrence of the sharp increase in current–characteristic of tip-breakage, and for the sharp decrease in i_{cct}–characteristic of the tip-membrane contact (i.e., P_{APR}, to P_{IND} transition). The desired output of the tip-membrane approach sequence reflects the goals of the change detection algorithm and includes the following transitions from:

S_0: Nominal microcapillary tip, to
S_1: Tip-membrane contact (p_{IND}), or to
S_2: Broken microcapillary tip.

System tasks including: (i) initiating the tip-membrane approach sequence; (ii) processing a sequential set of time invariant observations, $y_{k,}$, at a sampling rate, f_s; (iii) monitoring the output signals of the threshold detection algorithm, d; and (iv) sending the instructions to the motion controller responsible for the motion of the tip with respect to the cell are monitored and initiated by the supervisory controller (Fig. 5).

B. Change Detection Algorithm

Data or observations are acquired in the basic form of discrete measurements

$$x_k = \theta_k + e_k \tag{2}$$

where x_k, the k^{th} observation in the process, is the raw measurement that includes the desired signal output θ_k and the additive noise signal e_k. The measurements are assumed to be a sequence of n independent, random variables $(x_k)_{1\leq k<n}$ with a mean value μ_i.

In this work, the mean value of i_{cct} is estimated using the cumulative moving average

$$\mu_i = \frac{1}{k+1}\sum_{k=1}^{n} x_{k+1} \tag{3}$$

and is updated after each sample k. Let μ_0 denote the particular value of the mean calculated from (3) during P_{APR}. At an unknown time t_0, i_{cct} will transition beyond a threshold. At time t_{alm}, following t_0, the shift is detected and an alarm is signaled indicating the transition from P_{APR} to P_{IND} (i.e., the tip-membrane contact) or tip-breakage has been detected. The requirements defined for monitoring i_{cct} is to detect when i_{cct} has exceeded the threshold minimizing the latency of the detection (i.e., minimizing $[t_{alm} - t_0]$), thus minimizing the indentation of the cell.

The P_{APR} to P_{IND} transition and breakage can be detected using the double-sided cumulative sum, or "cusum" [17]. The cusum provides the following two recursive statistics, also referred as decision functions, that are used to determine the signaling of a monitored change in i_{cct}

$$\begin{aligned} C_k^{+} &= \max\left[0, C_{k-1}^{+} + x_k - \mu_i - \lambda\right] \\ C_k^{-} &= \max\left[0, C_{k-1}^{+} - x_k + \mu_i - \lambda\right]. \end{aligned} \tag{4}$$

Both statistics provide information regarding the accumulation of residuals of the raw data from the mean (i.e., $x_k - u_i$, and $-x_{\downarrow}k + u_{\downarrow}(i,)$). C_k^{+} defines the decision function for positive accumulations, while C_k^{-} is the decision function for negative accumulations. The initial values for C_0^{+} and C_0^{-} are zero. λ, also known as the "slack" variable, is selected such that accumulations will occur when the residual is greater than the value of λ.

To increase the flexibility of the algorithm, and generalize the design amongst system variations (e.g., differences in system noise, slight variations in microcapillaries), (4) is normalized with-respect-to the standard deviation. The residual can be rewritten as

$$y_k = \frac{\pm(x_k - u_i)}{\sigma} \tag{5}$$

in C_k^{+} and in C_k^{-}, respectively. y_k is the normalized residual as a function of the observation x_k and the cumulative moving av-

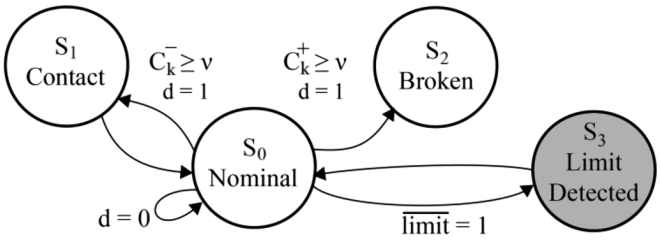

Fig. 6. The state diagram of the microcapillary tip-membrane approach sequence.

erage. The cusum in (4) can be rewritten in terms of the standard deviation

$$C_k^+ = \max\left[0, C_{k-1}^+ + y_k - \lambda\right]$$
$$C_k^- = \max\left[0, C_{k-1}^- - y_k - \lambda\right] \tag{6}$$

where λ is the slack variable chosen in terms of σ. The threshold, ν, is set to a multiple of σ

$$\nu = M\sigma \tag{7}$$

where M is a constant.

A detected change is defined by the following rule, where

$$d = \begin{cases} 0, & \text{if } C_k^+ < \nu \cap C_k^- < \nu \\ 1, & \text{if } C_k^+ \geq \nu \cup C_k^- \geq \nu \end{cases}. \tag{8}$$

A change in the decision is accepted when, $d = 1$, if the decision function, C_k^+ or C_k^- exceeds ν or rejected otherwise if $d = 0$. A state diagram illustrates the output from (8) and the states transitions from Section II-A (Fig. 6).

For the purposes of validating the algorithm, several rules were established. Tip-membrane contact detection, S_1, was defined when the C_k^- exceeds ν and p_{sc} exists between p_{VC} and p_D

$$S_1 : C_k^- \geq \nu \cap p_{VC} \leq p_{sc} < p_D. \tag{9}$$

A broken tip S_1 was defined when C_k^+ exceeds the threshold in the indentation region, where the position of the tip reaches the substrate

$$S_2 : C_k^+ \geq \nu \cap X \geq p_{VC} + h_C. \tag{10}$$

A false alarm occurs where either C_k^+ or C_k^- occurs prior to the tip reaching p_{VC}

$$FA : \left(C_k^+ \geq \nu \cup C_k^- \geq \nu\right) \cap X \leq p_{VC} \tag{11}$$

For full automation and online demonstrations, the state chart is illustrated (Fig. 6). A software limit condition $\overline{\text{limit}}$ represents the maximum tip position, which would signal the motion controller to halt in the event the tip exceeds a point dangerously close to the substrate. Establishing this limit is recommended during routine operation. For the purposes of this work, a limit has not been used to allow the possibility of all scenarios (e.g., tip-membrane contact detection, membrane rupture, and tip-breakage detection).

An estimate of the alarm time after the threshold is exceeded and is given by

$$t_{alm} = \min\left\{k : \left(C_k^+ \geq \nu\right) \cup \left(C_k^- \geq \nu\right)\right\}. \tag{12}$$

An estimate of the value of the new process mean value, μ_1, following the alarm, can be calculated for a tip-membrane contact detection [18]:

$$\mu_1 = \mu_0 - \frac{C_k^-}{N^-} - \lambda. \tag{13}$$

In SCE, (13) is of interest for the SCE routine given the decrease in i_{cct} from p_C and provides an estimate of the required potential for SCE to occur [5]. N^- is a counter that is incremented by one after each sample and reset to 0 when C_k^- equates to zero in (4). A thorough description of the cusum, applications and alternate variations of the algorithm can be found in [16] and [18]–[20].

C. System Parameter Acquisition

Adjusting the values of ν and λ obtain different performance results in the form of tip-membrane indentation distance. λ is typically chosen as half the value of the shift desired to be detected and a reasonable value of ν is 5σ [18]. Reference [20] provides some suggestions on tuning the parameters. Decreasing λ increases the rate of change of the cusum and increasing λ will reduce the number of false alarms. Tuning initial parameters by trial-and-error achieves satisfactory results, but may not provide the performance required. In this work, using an iterative process, offline data, and a wide range of ν and λ generate indentation distances based on the rules defined for the tip-membrane approach sequence. Using the results, a contour plot indicates the best combinations of ν and λ. Parameters, determined for the velocity of 1 μm/s, are subsequently used to generate parameters for higher velocities.

Combinations of ν and λ generated over large intervals will generate a contour plot (i.e., performance surface) of the indentation distances, $p_{SC} - p_{VC}$, as a function of ν and λ. A valid tip-membrane indentation occurs where (9) is valid. Tip-breakage is recorded where (10) is valid and a false alarm is recorded where (11) is valid. Parameter combinations of ν and λ that generate a false alarm or tip-breakage alarm are assigned a large value (e.g., 20 μm). This indentation value, not achievable using the cells in this work, is much greater than twice the value of the average cell height, $\overline{h}_c$. Assigning a high indentation depth value to parameters incurring a false alarm, no alarm, or tip-breakage provides a means for determining less suitable parameter combinations and maintains continuity of the performance surface.

Where the sampling rate of y_k remains constant, some increase to the tip-velocity can be facilitated by reducing the number of samples elapsed before an alarm is generated (i.e., shift from μ_1 to μ_0 systems). However, similar parameters for lower velocities will likely not provide the response required. An approximation of the number of samples elapsed

before a sample diverges from μ_0 to μ_1 is known as the average-run-length (ARL). The ARL is the estimated number of samples before a sample transitions from the in-control (IC) state to the out-of-control (OC) state. The P_{APR} represents the IC state and P_{IND} represents the OC state. The ARL for a single-sided cusum for a shift of $\mu_1 - \mu_0$ can be approximated in terms of σ using [21]

$$\mathrm{ARL} = \frac{e^{-2\psi(\nu+1.166)} + 2\psi(\nu + 1.166) - 1}{2\psi^2} \tag{14}$$

where $\psi = \mu_1 - \mu_0 - \lambda$ for ARL^+ in the positive cusum and $\psi = (-(\mu)_1 - \mu_0) - \lambda$ for ARL^- in the negative cusum calculation. The following provides the approximation for double-sided cusum ARL:

$$\frac{1}{\mathrm{ARL}} = \frac{1}{\mathrm{ARL}^-} - \frac{1}{\mathrm{ARL}^+}. \tag{15}$$

Further discussion of (14) and (15) are found in [18] and [21]. The $\mathrm{ARL}_{1(\mu\mathrm{m/s})}$ is determined using the performance surface and offline data a nominal velocity of 1 μm/s. In this work, the ARL for proportional increases in velocity is determined using a reverse lookup table generated with (15) and a simple relationship

$$\mathrm{ARL}_{x\frac{um}{s}} = \mathrm{ARL}_{1\frac{\mu m}{s}} \left(\frac{1\frac{\mu m}{s}}{x\frac{um}{s}} \right) \tag{16}$$

where x represents the tip velocity.

D. Algorithm Evaluation

The inherent challenge in many automated techniques involving the delivery of molecules using out-of-plane (OOP) [22] methods is the lack of useful visual data to provide a distance relationship between the tip and the cell membrane. This is a common challenge when using methods of delivery by a microcapillary descending on the surface of a cell membrane by intracytoplasmic/pronuclear injection [11] or by SCE [1], [3] when using conventional methods of microscopy. Adhered cells are manipulated and analyzed while attached to a substrate. Therefore, resolving the tip-membrane distance using cells with a small h_C combined with automation techniques using the top-down delivery method described in [1] and [3] is nontrivial. Yet, in order to validate the algorithm, the visual data (i.e., determining p_{VC}) must be related to i_{cct}. Therefore, the following experimental goals were defined to demonstrate the proposed algorithm.

1) Visually estimate the distance between the tip and the cell membrane using manual image analysis and correlate this tip-membrane distance with i_{cct}, and position encoder data.
2) Estimate the location of p_{VC} for each cell.
3) Using a range ν and λ, determine when p_{SC} is detected, and acquire the indentation depth $(p_{SC} - p_{VC})$.
4) Test the cusum algorithm online with the most efficient ν and λ.
5) Test the cusum algorithm online using with higher than the nominal tip-approach velocities.

III. Experimental Setup

The experimental setup is required to provide an estimate of and correlate the tip-membrane distance, using the top-down method of tip-placement [1], [3], with the electrical feedback of the SCE circuitry. The setup can be subdivided into the electrical data acquisition system, the optical data acquisition system called the multiaxis optical train, a postprocessing interface developed using NI LabVIEW 11.0, and finally the robotic-assisted cell manipulation platform described in [1].

A. Experimental Apparatus

1) Electrical Data Acquisition System: The data acquisition system consists of the Axoporator 800A Single-cell Electroporator. The Axoporator outputs a fixed 100 Hz low potential, bipolar square wave signal representative of the current through the microcapillary. The resulting signal is low-pass filtered $(f_c = 3.5\ \mathrm{kHz})$ to remove the capacitive transient of the system prior to passing the signal to an analog-to-digital encoder (NI USB-6009 DAQ). The DAQ subsamples the peak-to-peak output of the Axoporator at 10 kHz before being passed to the main algorithm.

SCE Microcapillaries were fabricated on a Sutter P-97 with borosilicate capillary glass (outer diameter 1.5 mm, inner diameter 1.1 mm) using the "Bee Stinger" protocol [23]. The microcapillaries were filled with 3 μL of 200 mM KCl. The microcapillary electrode consisted of a 0.25 mm diameter, 0.9999 ultrapure, annealed silver wire coated with silver-chloride placed in contact with the KCl in the tip of the microcapillary.

2) Multiaxis Optical Train: An inverted, differential interference contrast (DIC), vertical optical train $(\mathrm{O_V})$ consists of a 40X objective (NA 0.6) and a 12-bit CCD camera. The $\mathrm{O_V}$ can simultaneously image both the microcapillary tip and the cross section of a cell on a prepared coverslip mounted at 90° to the horizontal plane in a custom built cell container. This was sufficient for tip-membrane proximity measurements as the tip approached the cell. This method of tip-placement is consistent with the relative motion between the tip and the membrane required by top-down, automated SCE [1], [3].

A custom horizontal optical train, $\mathrm{O_H}$, [Fig. 7(a)], was designed to accurately align the tip with h_C on the axis perpendicular to the optical axis of the $\mathrm{O_V}$. Aligning the tip to the cell nucleus provides a suitable target for automated SCE. The $\mathrm{O_H}$ provided LED illumination and was focused on the cell using a lens pair with 50 mm focal lengths. The objective consisted of a 20X (NA 0.45) which was focused at 200 mm onto the sensor of a second 12-bit CCD camera.

3) Cell Container Assembly: The format of the cell container was designed such that both optical trains allowed visibility and image acquisition without disturbing the cell container or microcapillary tip [Fig. 7(b)]. The cell container gasket was fabricated by machining a two-layer mold out of Delrin and filling the mold with PDMS. The mold and PDMS was heated and allowed to cure overnight. The PDMS cell container gasket was then rinsed thoroughly with distilled water, followed by a 70% ethanol (EtOH) rinse and then allowed to dry.

The outer No. 1 glass coverslips acted as viewing windows [Fig. 7(c)]. The coverslips were cut to size by scoring each side using a carbon graphite pen and separating the coverslip into two rectangular pieces. The coverslips were cleaned with EtOH

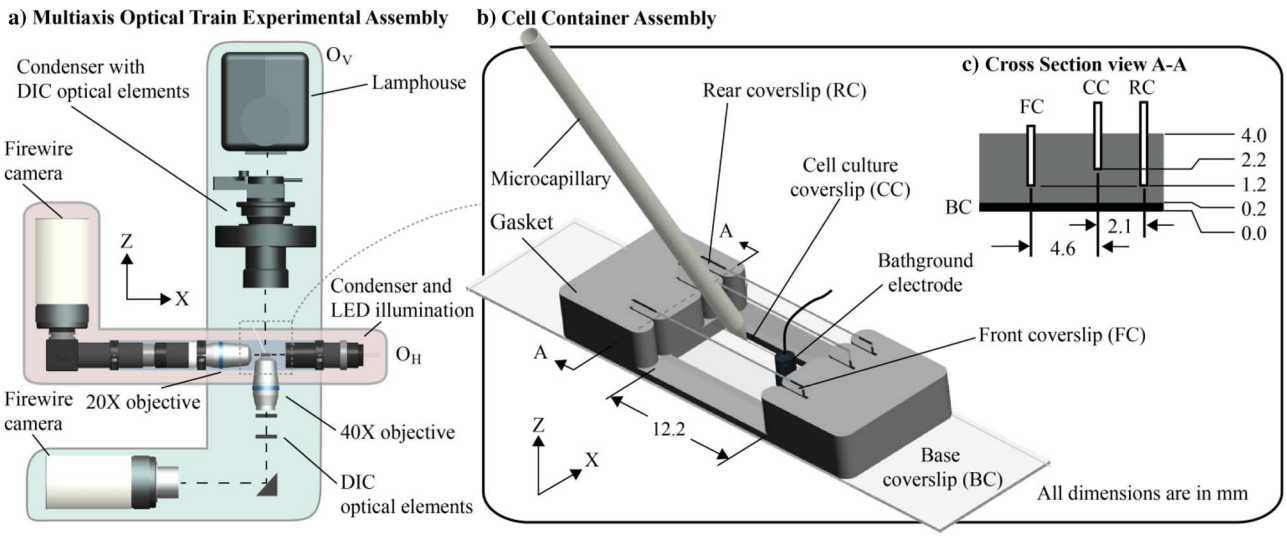

Fig. 7. (a) The multiaxis optical train and gasket assembly. (b) The cell container assembly allows the same cell to be effectively viewed on the vertical (O_V) and horizontal optical (O_H) trains, while manipulating the cells. The gasket, rear, front, and base coverslip provide a seal to contain the media needed for cell viability during experimentation. The front and rear coverslip provide a sufficient optical interface for light transmission on O_H. (c) The bottom edge of the cell culture coverslip is raised 1 mm higher above the bottom edge of the front and rear coverslips to minimize optical artifacts on O_H occurring at the cell culture coverslip.

and placed directly in the appropriate slot in the gasket which was set on a No. 1.5, 12.5 × 50 mm coverslip. The cell container was allowed to dry completely in a biosafety cabinet.

B. Cell Culture and Cell Coverslip Preparation

NIH/3T3 cells (ATCC #CRL-1658) were prepared using culture media composed of 10% fetal bovine serum, and 1% penstrep in α-Modified Eagle Medium (αMEM). Cells were cultured in 60 mm Petri dishes for 48 hours until the cells were approximately 90% confluent.

The cell culture coverslip was prepared in the same manner as the outer coverslips, but was allowed to dry inside a 30 mm Petri dish. Upon subculturing cells, 2.0 mL of culture media and 0.5 mL of cell solution were placed in each 30 mm dish with the cell culture coverslip. The cells were then incubated for 7 hours prior to experimentation.

C. Experimental Procedure

In order to satisfy the experimental goals outlined in Section II, the experimental procedure was executed in two stages including: (i) the offline testing and the data analysis followed by (ii) the online algorithm demonstrations.

A series of offline tests were conducted using raw data collected from 40 tip-membrane approach sequences. This data was used to correlate the image data (e.g., tip-membrane distance) with the measurements of i_{cct}–a procedure that has yet to be validated in the tip-placement procedure prior to SCE. Secondly, the cusum algorithm was evaluated using a range of ν and λ.

Following the offline analyses, 16 online experimental tip-membrane approach sequences were performed using parameters that were determined from the offline tests. The goal of the online tests was to demonstrate the performance of the algorithm in the same manner as would be performed in a routine automated SCE tip-membrane placement sequence, while validating the image data with the i_{cct} feedback.

1) Offline Data Collection: Following the 7-hour incubation period, the glass coverslip was removed from the media with sterile tweezers. The cell-side of the coverslip was placed in the cell container slot facing the tip. The cell container was then filled with 330 μL of transparent αMEM (no phenol red) and gently tapped to distribute the media.

The alignment procedure began by placing the cell container assembly on the robotic stage [Fig. 1(a)]. The bath ground electrode was lowered into the container on the tip side without disturbing the cell culture coverslip. The bottom edge of the cell culture coverslip was maneuvered into the field-of-view (FOV) of the O_V using the automated platform. The bottom edge of the coverslip was brought into focus and a random cell on the cell culture coverslip was selected for analysis. The robotic stage moved $+500$ μm on the X axis from the microcapillary side allowing room to submerse the tip into the container. The microcapillary, mounted at a 30° angle relative to the cell coverslip, was lowered into the cell container and brought into focus with the FOV of O_V. The cell culture coverslip was maneuvered back to the original position and the tip was aligned to h_C on the Y axis, approximately 30 μm away from the substrate [Fig. 1(b)]. The O_H was then positioned such that the cell coverslip (cell side) was in the focal plane and the microcapillary tip and target cell were within the FOV. The tip was finally aligned on the Z axis with the centroid of the nucleus [see Fig. 1(c)] by alternating the cell and the tip into the focal plane and making minor adjustments to the tip position. This ensured the tip contacted h_C during the automated tip-membrane placement procedure. Without the O_H, alignment of the tip to h_C is inaccurate and frequently results in the tip missing h_C. Following the alignment procedure, the automated tip-membrane placement sequence began. The alignment procedure, which occurs prior to the automated tip-membrane placement sequence,

was performed manually. An experienced operator completed the alignment procedure within approximately 5 minutes.

After alignment, data collection was initiated and the stage moved the cell toward the microcapillary tip at a constant rate of 1 μm/s. The sampling rate for i_{cct} was 25 Hz, while the image acquisition was performed at 10 fps at full resolution (1392 $\times$ 1040 pixels). This provided a position-image resolution of 0.10 μm per frame during motion of the tip. Data including: i_{cct}, a time stamp, the encoder position and an image number were simultaneously stored to a file for post processing and cross-referencing. Data collection stopped as soon as the microcapillary tip intentionally contacted and broke on the glass substrate displaying the characteristic sharp increase in current signaling the end of the raw data collection sequence. Each cell culture coverslip was used once and the procedure took less than 15 minutes from the time the cell coverslip was removed from the Petri dish in the incubator.

2) Online Algorithm Evaluation: 16 online tests were used to demonstrate the performance of the cusum using the same experimental setup as in the offline tests. However, in contrast to the offline experimentation, the goal was to stop the advance of the microcapillary upon tip-membrane contact detection and return the tip to the starting position. Tip-approach velocities of 1, 2, 4, and 8 μm/s were used and four experimental trials of each approach velocity were performed.

3) Raw Data Analysis and the LabVIEW Interface: A LabVIEW interface was developed to analyze the results of the offline and online data (Fig. 9). The interface displayed the raw output of i_{cct}, μ_i, C_k^+, C_k^-, and d. The LabVIEW Vision algorithm, "Highlight Details," was used to improve the contrast of the tip and the membrane outline. The contact between the cell membrane and the tip p_{VC} was estimated when the outline of the tip touched the outline of cell membrane. It was estimated that the tip-membrane contact could be determined with an average error of ± 0.7 μm.

IV. Results and Discussion

A. Offline Test Results and Statistical Data Analysis

In order to obtain h_c for each cell, pixel-to-μm conversion measurements were made from the substrate surface to the tip-membrane contact point of the microcapillary, h_C, using images acquired from the O_V [e.g., the images in Fig. 1(b) and d)]. The mean height of the cells, $\overline{h_C}$, was 7.2 μm ($SD = 1.5$ μm, N_{56}).

An example of the tip-membrane approach sequence is provided in detail next and illustrates the raw data that was collected for the offline data analysis and for the evaluation of the cusum algorithm (Fig. 8). The estimate for σ, used in (1), (5), and (7) is acquired during each P_{APR}, where i_{cct} is constant and is obtained when the tip is in motion a distance of 30 μm from the glass substrate. In this example $\sigma = 0.0012$ μA and the offline average was determined to be $\overline{\sigma} = 0.0012$ μA ($SD = 0.0002, N = 40$). The accumulated average, μ_0, and raw data are shown in detail before and after p_{VC} ($k = 744$) in a magnified window [Fig. 8(b)]. As the tip approaches p_{VC}, i_{cct} measurements begin to decrease below the level $\mu_0 - \lambda$, and is reflected on the cusum C_k^-. After the tip moves beyond p_{VC} and indents the cell, i_{cct} decreases steadily during P_{IND}. As the tip continues to indent the cell, C_k^- increases steadily as

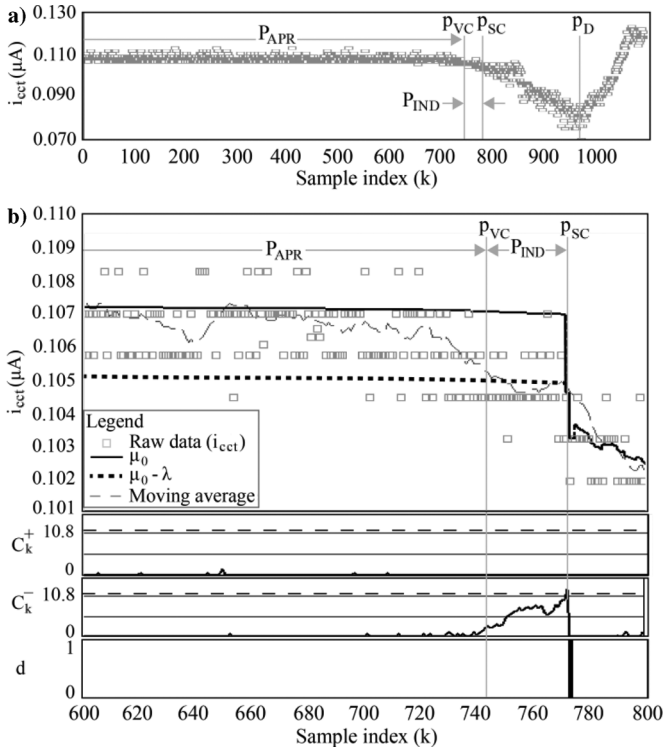

Fig. 8. Offline experimental test output. (a) The complete raw data set used for post analysis. (b) In the region between $k = 600$ and 830, the statistic C_k^- is observed to increase rapidly near p_{VC}. Measurements exceeding $\mu_A \pm \lambda$ an increase in C_k^+ and C_k^- occurs, respectively ($\mu_A - \lambda$ is shown). Shortly after, d evaluates to 1 when $C_k^- \geq v$ at $k = 772$ (p_{SC}) or approximately 1.07 μm after p_{VC} (21% of indentation). In this example, $\nu = 10.8\sigma$, $\lambda = 1.6\sigma$ and was determined to be $\sigma = 0.001$ μA. The trend of the raw data is shown with the moving average (window size is 16).

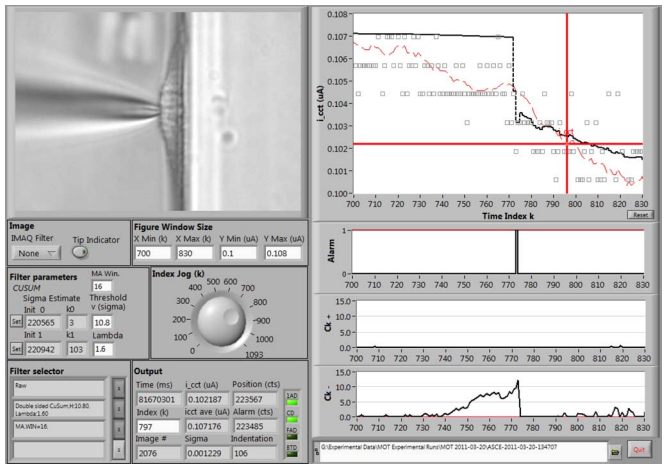

Fig. 9. The LabVIEW graphical user interface. The LabVIEW graphical user interface was used to cross-reference and analyze i_{cct} and tip-membrane position data and observe the output of the cusum algorithm.

the raw measurements of i_{cct} grow further from μ_0. C_k^- then exceeds the threshold ($\nu = 10.8\sigma$), d evaluates to 1 ($k = 772$) and an alarm is signaled indicating p_{SC}. Finally, the end-point signal of the offline tip-membrane approach occurs when the micropipette reached the bottom of the cell on the glass substrate. The tip breaks and the abrupt increase in current is observed [$k > 974$ in Fig. 8(a)]. The trend of the raw measurements is

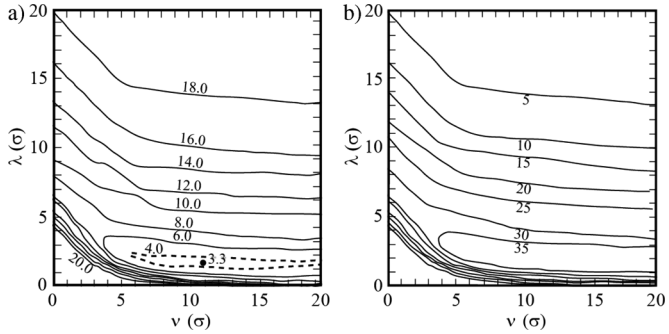

Fig. 10. The performance surface (contour units are in μm). (a) The performance plot was generated using the 40 tip-membrane sequences and an approach velocity of 1 μm/s. In (b), a contour plot indicates the number of tip-membrane approach sequences that generated a valid indentation value of $(p_{SC} - p_{VC})$ satisfying (9). The minimum occurred at $\nu = 10.8\sigma$ and $\lambda = 1.6$, N $= 38$. The average indentation depth of the 38 valid tip-membrane sequences was 2.4 μm.

illustrated using a moving average filter with a window size of 16.

Following the data collection of the tip-membrane approach sequences for the offline analysis, a performance surface plot was generated for ν and λ for each of the 40 tip-membrane approach sequences. The population average of the 40 performance surfaces is shown in Fig. 10(a) for parameters within $[0\sigma, 20\sigma]$ at a resolution of 0.2σ. Smaller indentation depths indicate a better selection of parameter pairs. A region where the performance surface indicates the lowest indentation values is shown in a dashed line in Fig. 10(a). Outside this boundary, significantly reducing λ rapidly leads to a greater number of false alarms due to the noise, where the cusum exceeds the threshold prematurely before p_{VC}. Increasing λ gradually increases the number of samples before an alarm condition occurs, which also reduces the rate of increase of the cusum. Therefore, the effects of both the noise and abrupt changes are less likely to create an alarm condition before the possibility of tip-substrate contact and cell destruction creating a significantly large increase in i_{cct}. Decreasing ν significantly increases the number of false detections given the short threshold to achieve. Increasing ν gradually increases the number of samples (i.e., distance) before the tip-membrane detection is met. ν is limited by the current drop available prior to the striking the substrate.

The minimum value of Fig. 10(a) occurred where $\nu = 10.8\sigma$ and $\lambda = 1.6\sigma$ with 38 offline tip-membrane sequences recorded providing an indentation value within the conditions in (9). The number of tip-membrane approach sequences that produced an alarm representing a successful tip-membrane contact detection where the condition $p_{VC} \leq p_{sc} < p_D$ is met is shown in Fig. 10(b). The average tip-membrane indentation value at $\nu = 10.8\sigma$ and $\lambda = 1.6\sigma$ was determined to be 2.4 μm excluding the 20 μm value assigned to two tip-membrane sequences producing broken tip signals. This corresponds to an average of 33% indentation depth (Fig. 3) before the tip-membrane contact is detected and an average tip-membrane contact detection occurring when $i_{cct}/(i_{cct})_{VC}$ is reduced to 96.8% after v_{PC} (Fig. 4).

TABLE I
AVERAGE-RUN-LENGTH (ARL) VALUES FOR SELECTED PARAMETERS

Velocity (μm/s)	ν (σ)	λ (σ)	ARL OC (samples)	ARL IC (samples)
1	10.8	1.6	24	4.16×10^{15}
2	10.8	1.1	12	5.60×10^{10}
4	5	1.1	6	1.61×10^{5}
8	2.4	1.1	3	526

TABLE II
ONLINE DEMONSTRATIONS RESULTS

#	V (μm/s)	ν (σ)	λ (σ)	Hc (μm)	Psc - Pvc (μm)	Ind. Ratio (%)
1	1	10.8	1.6	6.9	1.4	20.5
2	1	10.8	1.6	7.9	4.8	60.5
3	1	10.8	1.6	5.5	1.1	19.3
4	1	10.8	1.6	8.5	2.1	24.3
5	2	10.8	1.1	5.7	2.6	44.5
6	2	10.8	1.1	7.7	3.0	38.5
7	2	10.8	1.1	5.7	3.3	58.6
8	2	10.8	1.1	5.4	1.1	19.8
9	4	5	1.1	8.0	0.8	9.7
10	4	5	1.1	7.5	1.8	23.8
11	4	5	1.1	9.0	2.9	32.1
12	4	5	1.1	7.0	1.8	25.4
13	8	2.4	1.1	5.0	1.6	31.7
14	8	2.4	1.1	6.1	1.6	26.4
15	8	2.4	1.1	4.2	0.9	22.2
16	8	2.4	1.1	6.7	0.8	11.4
				Ave.	2.0	29.3
				SD	1.1	14.7

The ARL calculated for $\nu = 10.8\sigma$ and $\lambda = 1.6\sigma$ using (15) is 24 samples or approximately 1 μm at a sampling rate of 25 Hz at the nominal velocity of 1 μm/s. The average shift in the mean, prior to contact detection was determined to be -2.05σ $(SD = 0.16, N = 38)$. Using (15), and the experimentally determined values of ν, λ, and a shift of -2.05 σ a table of ARL values was generated. Parameters ν, and λ for 2, 4, and 8 μm/s were selected according to (16) and listed in Table I.

Entering a value of $\delta^- = 0$ (i.e., no shift in μ_1) for the selected parameter pairs provides an approximation for the ARL for the IC process during P_{APR}. Higher ARL values for the IC condition have a higher tolerance to noise thus reducing false alarms.

B. Online Algorithm Evaluation

Table II summarizes the results of the 16 fully automated tip-membrane placement sequences used to demonstrate the online performance of the cusum algorithm. In 100% of all consecutive sequences using the experimentally determined parameters, the algorithm was successful in detecting the tip-membrane contact and the cell remained viable after the tip-membrane placement sequence. On average, the indentation depth was 2.0 μm $(SD = 1.1, N = 16)$ and the indentation depth was 29.3% $(SD = 14.7, N = 16)$.

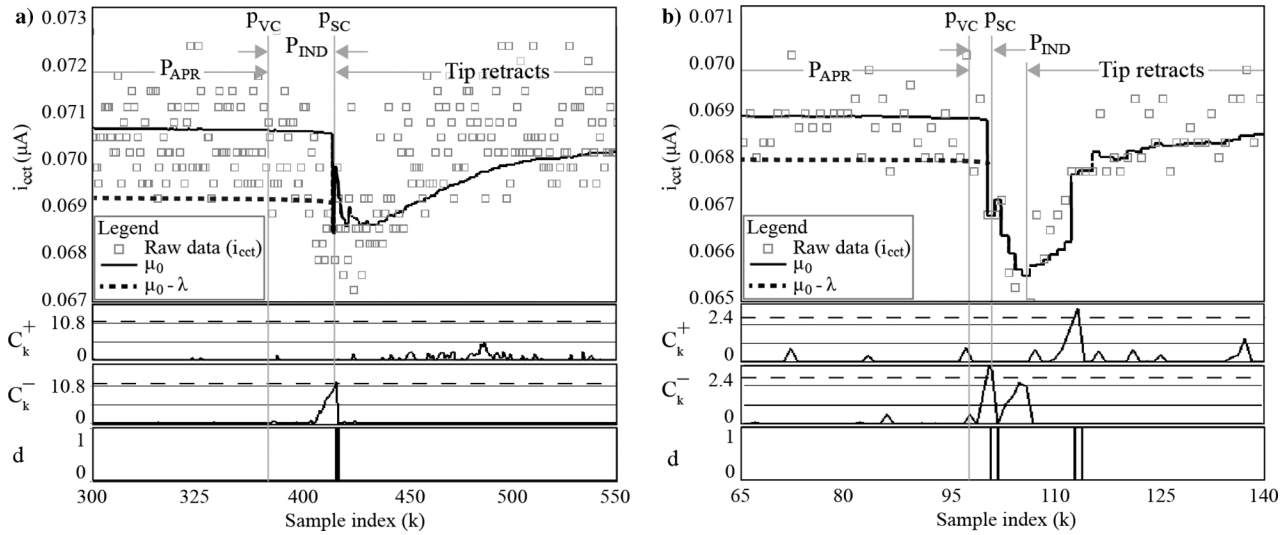

Fig. 11. Examples of the online cusum demonstrations. (a) The i_{cct} output during a tip-placement *Sequence 1* (1 μm/s). (b) The i_{cct} output during a tip-placement *Sequence 13* (8 μm/s). In both sequences, C_k^- exceeds ν signaling d to evaluate to 1 and the motion controller halts the advance of the tip. After a pause, the tip returns to the starting position causing i_{cct} to returns to the original levels prior to P_{IND}.

Two examples of the online tip-placement sequences, from Table II including: *Sequence #1* (1 μm/s) and *Sequence #13* (8 μm/s) are shown in Figs. 11(a) and (b), respectively. In each tip-membrane approach sequence during indentation, i_{cct} decreased nominally until C_k^- exceeded the threshold setting d to 1. The supervisory controller issued the command to the motion controller to halt and then retracted the tip to the starting position. During the tip-retraction, i_{cct} is observed to return to the original level before the tip-membrane procedure was initiated.

It is more apparent in Fig. 11(b) that choosing a lower λ and ν to accommodate shorter ARL at higher velocities is prone to a higher probability of false alarms caused by random noise spikes. The effect of random noise is increasingly observed in the cusum of Fig. 11(b) and nearly reaches half the value of ν. It is likely ν could be tuned to accommodate a higher tolerance at the expense of a greater number of samples before ν is exceeded. Further improvements to parameter selection could be made by implementing a learning algorithm into the routine, while performing automated SCE on a conventional system using a similar process, while estimating the location of p_C.

V. Conclusion

Automation of SCE is a powerful method for transfection that will elucidate new single cell assays requiring higher than manual throughput, increased accuracy and repeatability. Semiautomated [3] and fully automated [1] methods of SCE are described in literature. However, an absence of literature on fully automated SCE of thin cells reduces the generality of the technique, and requires further analysis. Consequently, little has been done in terms of exploring the automation of the tip-placement sequence and tip-membrane contact detection for thin cells in electrode-based, robotic-assisted platforms. Early detection of tip-membrane contact is necessary to prevent the destruction of the tip or the cells and improve the overall efficiency in automated SCE.

This work has demonstrated a fully automated method for tip-membrane contact detection based on the cumulative-sum, "cusum." This algorithm was generalized for tip-membrane contact detection for thin or thick cells and can be adopted by systems employing fully automated microcapillary-based SCE in the presence of system noise common to electrode-based measurements. Furthermore, this work validated for the first time, a comparison of the current through the electrode with image-based, distance measurements of the microcapillary tip relative to the cell membrane using thin adhered mammalian cells.

Acknowledgment

The authors would like to express their gratitude to Prof. T. Beischlag, SFU Faculty of Health Sciences, for the use of their facilities and for providing training in biotechniques.

References

[1] K. Sakaki, N. Dechev, R. D. Burke, and E. J. Park, "Development of an autonomous biological cell manipulator with single cell electroporation and visual servoing capabilities," *IEEE Trans. Biomed. Eng.*, vol. 56, no. 8, pp. 2064–2074, Aug. 2009.

[2] K. Sakaki, I. G. Foulds, W. N. Liu, R. D. Burke, N. Dechev, and E. J. Park, "RoboSCELL: An automated single cell arraying and analysis instrument," *Biomed. Microdevices*, vol. 11, pp. 1317–1330, 2009.

[3] C. Bae and P. Butler, "Automated single-cell electroporation," *Biotechniques*, vol. 41, pp. 399–402, 2006.

[4] K. Haas, W. C. Sin, A. Javaherian, Z. Li, and H. T. Cline, "Single-cell electroporation for gene transfer *in vivo*," *Neuron*, vol. 29, pp. 583–591, 2001.

[5] J. L. Rae and A. Levis, "Single-cell electroporation," *Pflugers Arch., Eur. J. Physiology*, vol. 443, no. 4, pp. 664–670, 2001.

[6] P. Lovell, S. H. Jezzini, and L. L. Moroz, "Electroporation of neurons and growth cones in *Aplysia Californica*," *J. Neurosci. Methods*, vol. 115, pp. 114–120, 2006.

[7] C. Ionescu-Zanetti, A. Blatz, and M. Khine, "Electrophoreses-assisted single-cell electroporation for efficient intracellular delivery," *Biomed. Microdevices*, vol. 10, pp. 113–116, 2007.

[8] I. Zudans, A. Agarwal, O. Orwal, and S. G. Weber, "Numerical calculations of single-cell electroporation with an electrolyte-filled capillary," *Biophy. J.*, vol. 92, pp. 3696–3705, 2007.

[9] Y. H. Anis, M. R. Hall, and D. R. Meldrum, "Automated selection and placement of single cells using vision-based feedback control," *IEEE Trans. Autom. Sci. Eng.*, vol. 7, no. 3, pp. 598–606, Jul. 2010.

[10] Y. Sun and B. J. Nelson, "Biological cell injection using an autonomous microrobotic system," *Int. J. Robot. Res.*, vol. 21, pp. 861–868, 2002.

[11] P. Kallio, T. Ritala, M. Lukkari, and S. Kuikka, "Injection guidance systems for cellular microinjections," in *Proc. IEEE/RAS Conf. Biomed. Robot. Biomechatronics*, 2006, pp. 696–701.
[12] Y. L. Zhang, M. L. Han, J. Vidyalakshmi, C. Y. Shee, and W. T. Ang, "Automatic control of mechanical forces acting on cell biomembranes using a vision-guided microrobotic system in computer microscopy," *J. Microscopy*, vol. 236, pp. 70–78, 2009.
[13] *The Axon Guide—A Guide to Electrophysiology & Biophysics Laboratory Techniques*. Sunnyvale, CA, MDS Analytical Technologies, 2008.
[14] M. J. Mousavi and K. L. Butler-Purry, "Detecting incipient faults via numerical modeling and statistical change detection," *IEEE Trans. Power Delivery*, vol. 25, no. 3, pp. 1275–1283, Jul. 2010.
[15] J. P. Royston and R. M. Abrams, "An objective method for detecting the shift in basal body temperature in women," *Biometrics*, vol. 36, pp. 217–224, 1980.
[16] M. Basseville and I. V. Nikiforov, *Detection of Abrupt Change. Theory and Applications*. Englewood Cliffs, NJ: Prentice-Hall, 1993.
[17] E. S. Page, "Continuous inspection schemes," *Biometrika*, vol. 41, pp. 100–115, 1954.
[18] D. C. Montgomery, *Introduction to Statistical Quality Control*, 4th ed. New York: Wiley, 2001.
[19] J. O. Westgard, T. Groth, T. Aronsson, and C. de Verdler, "Combined Shewhart-cusum control chart for improved quality control in clinical chemistry," *Clin. Chem.*, vol. 23, pp. 1881–1887, 1977.
[20] F. Gustaffsson, *Adaptive Filtering and Change Detection*. New York: Wiley, 2000.
[21] D. Siegmund, *Sequential Analysis: Tests and Confidence Intervals*. New York: Springer-Verlag, 1985.
[22] H. Huang, D. Sun, J. K. Mills, W. J. Li, and S. H. Cheng, "Visual-based impedance control of out-of-plane cell injection systems," *IEEE Trans. Autom. Sci. Eng.*, vol. 6, no. 3, pp. 565–571, Jul. 2009.
[23] *P-1000 & P-97 Pipette Cookbook Revision E,*. Novato, CA, Sutter Instrument, 2009.

Kelly Sakaki received the Telecommunications Engineering Diploma from the Northern Alberta Institute of Technology, Edmonton, Canada, in 2001, the B.Eng. degree in computer systems engineering and the M.A.Sc. degree in mechanical engineering from the University of Victoria, Victoria, BC, Canada, in 2005 and 2007, respectively. Currently, he is completing a Ph.D. degree in the Department of Mechatronic Systems Engineering, School of Engineering Science, Simon Fraser University, Burnaby, BC, Canada.

His research interests include automation, biorobotic, electronic and mechanical systems design, single cell analysis, single cell biomanipulation using localized electroporation techniques and machine vision.

Hadi Esmaeilsabzali received the B.A.Sc. degree in biomedical engineering from the School of Medicine, Shahid Beheshti University of Medical Sciences, Tehran, Iran, in 2003, and the M.A.Sc. degree in control engineering from the School of Electrical Engineering, Iran University of Science and Technology, Tehran, in 2006. Since 2009, he has been working towards the Ph.D. degree in the Department of Mechatronic Systems Engineering, Simon Fraser University, Burnaby, BC, Canada.

His research interests include immunomagnetic cell manipulation, development of lab-on-a-chip Bio-MEMS for rare-cell detection, isolation, characterization, and point-of-care testing (POCT) devices, single-cell biomanipulation, and machine vision applied to these areas.

Nikolai Dechev (M'03) received the B.A.Sc., M.A.Sc., and Ph.D. degrees from the Department of Mechanical Engineering, University of Toronto, Toronto, ON, Canada, in 1996, 1999, and 2004, respectively.

He is currently an Associate Professor of Mechanical Engineering at the University of Victoria. His research interests include (1) biomedical systems design in the areas of advanced hand prosthesis, implantable sensors and prosthesis control, (ii) MEMS (microelectromechanical systems) sensors, and (iii) robotic micromanipulation and automation technologies for MEMS and biological cells.

Prof. Dechev is a member of the American Society of Mechanical Engineers (ASME).

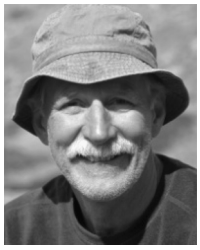

Robert D. Burke received the B.Sc. (Hon) degree and the Ph.D. degree from the University of Alberta, Edmonton, Canada, in 1974 and 1978, respectively.

He has been with the University of Victoria since 1980, and is currently Chair of the Department of Biochemistry and Microbiology. His research interests are in cellular and developmental biology. He has published over 100 journal papers in these areas.

Edward J. Park received the B.A.Sc. degree from the University of British Columbia, Vancouver, BC, Canada, in 1996, and the M.A.Sc. and Ph.D. degrees from the University of Toronto, Toronto, ON, Canada, in 1999 and 2003, respectively, all in mechanical engineering.

He is currently an Associate Professor of Mechatronic Systems Engineering at the Simon Fraser University, where he is also the Director of the Biomechatronic Systems Laboratory. Previously, he was an Assistant Professor at the Department of Mechanical Engineering, University of Victoria, Canada, from 2003 to 2008. His current research interests include: (i) biomechatronics and biomedical technologies for life sciences, rehabilitation and medicine and (ii) mechatronics applied to next generation vehicular, robotic and space systems. He has authored or coauthored close to 100 journal and conference papers in these areas.